Multipoint formulas in inverse problems and their numerical implementation

Roman Novikov, Vladimir Sivkin, Grigory Sabinin

▶ **To cite this version:**

Roman Novikov, Vladimir Sivkin, Grigory Sabinin. Multipoint formulas in inverse problems and their numerical implementation. Inverse Problems, 2023, 39 (12), pp.125016. 10.1088/1361-6420/ad06e6 . hal-04053473

HAL Id: hal-04053473
https://hal.science/hal-04053473v1

Submitted on 31 Mar 2023

HAL is a multi-disciplinary open access archive for the deposit and dissemination of scientific research documents, whether they are published or not. The documents may come from teaching and research institutions in France or abroad, or from public or private research centers.

L'archive ouverte pluridisciplinaire **HAL**, est destinée au dépôt et à la diffusion de documents scientifiques de niveau recherche, publiés ou non, émanant des établissements d'enseignement et de recherche français ou étrangers, des laboratoires publics ou privés.

Multipoint formulas in inverse problems and their numerical implementation

R.G. Novikov, V.N. Sivkin, G.V. Sabinin

March 31, 2023

Abstract

We present the first numerical study of multipoint formulas for finding leading coefficients in asymptotic expansions arising in potential and scattering theories. In particular, we implement different formulas for finding the Fourier transform of potential from the scattering amplitude at several high energies. We show that the aforementioned approach can be used for essential numerical improvements of classical results including the slowly convergent Born-Faddeev formula for inverse scattering at high energies. The approach of multipoint formulas can be also used for recovering the X-ray transform of potential from boundary values of the scattering wave functions at several high energies. Determination of total charge (electric or gravitational) from several exterior measurements is also considered. In addition, we show that the aforementioned multipoint formulas admit an efficient regularization for the case of random noise. In particular, we proceed from theoretical works [Novikov, 2020, 2021].

Keywords: inverse scattering, charge recovery, multipoint formulas, numerical implementation
AMS subject classification: 35J10, 35P25, 35R30, 65N21, 78A46, 81U40

1 Introduction

Many functions of potential theory, scattering theory, and other fields admit asymptotic expansions of the form

$$z(s) = \sum_{j=1}^{N} \frac{a_j}{s^{j-1}} + \mathcal{O}(s^{-N}), \text{ as } s \to +\infty, \tag{1.1}$$

where $s \in (\sigma, +\infty)$, for some $\sigma > 0$, and a_j are complex numbers; see, for example, [1], [21], [22], [27], [28], [32], [38]. In addition, in some cases, the most important information is contained in a_1 (and/or some next leading coefficients), whereas $z(s)$ is measured in several points $s \in (\sigma, +\infty)$. In the present work we continue studies of [27], [28] on finding a_1 from $z(s)$, given at several sufficiently large s, with applications to inverse scattering at high energies. We also consider determination of total charge (electrical or gravitational) from measurements at several remote points. For other applications of such studies to phased and phaseless inverse scattering, see [27], [32].

One of the most essential results of the present work consists in an efficient regularization of the formulas of [27] for finding a_1 from z at several points in the presence of random noise; see Sections 2, 5, 6, 7. This regularization opens perspectives for practical applications where data are always noisy.

In particular, we consider the stationary Schrödinger equation

$$-\Delta\psi + v(x)\psi = E\psi, \quad x \in \mathbb{R}^d, \quad E > 0, \tag{1.2}$$

where

$$v \text{ is compactly supported and sufficiently regular on } \mathbb{R}^d. \tag{1.3}$$

For equation (1.2), we consider the scattering solutions $\psi^+ = \psi^+(x,k)$, $k \in \mathbb{R}^d$, $k^2 = E$, specified by

$$\psi^+(x,k) = e^{ikx} + \frac{e^{i|k||x|}}{|x|^{(d-1)/2}} f_1\left(k, |k|\frac{x}{|x|}\right) + \mathcal{O}\left(\frac{1}{|x|^{(d+1)/2}}\right) \quad \text{as } |x| \to +\infty, \tag{1.4}$$

uniformly on $x/|x|$. The coefficient f_1 arising in (1.4) is the scattering amplitude for equation (1.2). The function f_1 at a fixed energy E is defined on

$$\mathcal{M}_E = \{k, l \in \mathbb{R}^d : \ k^2 = l^2 = E\} = \mathbb{S}^{d-1}_{\sqrt{E}} \times \mathbb{S}^{d-1}_{\sqrt{E}}. \tag{1.5}$$

For more information on direct scattering for equation (1.2), see, for example, [5].

We consider, in particular, polychromatic inverse scattering at high energies for equation (1.2), formulated as follows:

Problem 1. *Find v (or some information about v) from f_1 at several sufficiently large energies E.*

Let

$$\widehat{v}(p) = (2\pi)^{-d} \int_{\mathbb{R}^d} e^{ipx} v(x) dx, \quad p \in \mathbb{R}^d. \tag{1.6}$$

For some formulas, it is convenient to write f_1 as

$$\begin{aligned} &f_1(k,l) = c(d,|k|) f(k,l), \\ &c(d,|k|) := -\pi i (-2\pi i)^{(d-1)/2} |k|^{(d-3)/2}, \text{ for } \sqrt{-2\pi i} = \sqrt{2\pi} e^{-i\pi/4}. \end{aligned} \tag{1.7}$$

In particular, we have that

$$f(k,l) = \widehat{v}(p) + \mathcal{O}(E^{-1/2}), \quad p = k - l, \quad (k,l) \in \mathcal{M}_E, \quad E \to +\infty. \tag{1.8}$$

Formula (1.8) goes back to [4], [9] and is known as the Born-Faddeev formula at high energies; see also, for example, [26]. This formula gives the simplest method for inverse scattering at high energies for $d \geq 2$. In addition, formula (1.8) admits much more detailed versions, at least, for smooth v.

Let, for example, $v \in \mathcal{C}_c^\infty(\mathbb{R}^d)$, where $\mathcal{C}_c^\infty$ denotes compactly supported infinitely smooth functions. Then (see Proposition 3.4 of [22]):

$$f(k(s), l(s)) = \sum_{j=1}^{N} \frac{a_j(p,\omega)}{s^{j-1}} + \mathcal{O}(s^{-N}) \text{ as } s \to +\infty, \tag{1.9}$$

where

$$\begin{aligned} &k(s) = p + (E - p^2)^{1/2} \omega, \quad l(s) = E^{1/2} \omega, \quad E = E(s) = s^2, \\ &p \in \mathbb{R}^d, \quad p \cdot \omega = 0, \quad \omega \in \mathbb{S}^{d-1}, \end{aligned} \tag{1.10}$$

and

$$a_1(p,\omega) = \widehat{v}(p), \tag{1.11}$$

where $\widehat{v}$ is defined by (1.6). One can see that expansion (1.9) is of the form (1.1), and the most important information (in the framework of inverse scattering) is contained in a_1.

In particular, due to (1.9), (1.11), we have that

$$\widehat{v}(p) = f(k(s), l(s)) + \mathcal{O}(s^{-1}), \text{ as } s \to +\infty. \tag{1.12}$$

Formula (1.12) is a variation of formula (1.8). In a similar way with (1.8), formulas (1.12), (1.10) give a method for inverse scattering at high energies for $d \geq 2$ (for $d = 1$ these formulas can be used only for $p = 0$).

In inverse scattering, the main disadvantage of Born-Faddeev formulas like (1.8), (1.12) consists in their slow convergence for large energies. This convergence corresponds to $\mathcal{O}(s^{-1})$ in (1.12). In this connection, recently, the article [28] suggested

$$\begin{aligned} &\text{formulas for finding } \widehat{v}(p) \text{ up to } \mathcal{O}(s^{-n}) \text{ as } s \to +\infty \\ &\text{from } f(k,l) \text{ given at } n \text{ points } (k,l) = (k_1(s), l_1(s)), ..., (k_n(s), l_n(s)), \end{aligned} \tag{1.13}$$

where, for example,

$$\begin{aligned} &k_j(s) = k(s_j) = k(s + \tau_j), \quad l_j(s) = l(s_j) = l(s + \tau_j), \\ &s > 0, \quad 0 = \tau_1 < \tau_2 < ... < \tau_n, \end{aligned} \tag{1.14}$$

where $(k(s), l(s))$ are defined as in (1.10) and (1.12). Formulas (1.13) are recalled in details in Subsection 3.1.

The results of the present work include the first numerical implementation of the multipoint formulas of [27], [28] for finding a_1 in (1.1) from $z(s)$ given at several points s, with applications to inverse scattering at high energies via formulas (1.13). The results of the present work also include extension of formulas (1.13) to phaseless inverse scattering at high energies.

The results of the present work also include a variation of formulas (1.9)–(1.11) which is considerably more convenient for applications to inverse scattering at high energies. And we implement these more convenient formulas on inverse scattering numerically. See Subsections 4.1 and 7.2.

Note that the asymptotic of the scattering functions ψ^+ at high energies also reduces to an asymptotic of the form (1.1). In the present work we also explain in which way the multipoint approach can be applied to recovering the X-ray transform of the potential v from boundary values ψ^+ at several high energies. See Subsection 4.2.

For other important results given in the literature on inverse scattering problems, see, for example, [2], [6], [8], [10], [11], [12], [13], [16], [19], [20], [28], [30], [31], [33], [34], [35], [36], and references therein. In particular, we expect that the multipoint approach can be also applied to inverse scattering for the Newton equation; see [18], [25] for known results on this inverse scattering. We also expect that the multipoint approach can be applied to finding the Fourier transform of potential from the Faddeev scattering data h in complex domain at a fixed energy with applications to inverse boundary value problems; see [13], [24].

Natural directions for further research also include possible generalizations of asymptotics like (1.9), (4.1) for potentials v with discontinuities. Our preliminary numerical tests of reconstruction formulas of Subsection 4.1 and Section 5 give encouraging results in this connection.

We also consider an electrical or gravitational field with potential

$$U(x) = \int_D \frac{\rho(x')dx'}{|x-x'|}, \quad x \in \mathbb{R}^3, \tag{1.15}$$

where D is a bounded domain in $\mathbb{R}^3$. It is well-known that $sU(s\theta)$ admits multipole expansion of the form (1.1) with

$$a_1 = \int_D \rho(x)dx; \tag{1.16}$$

see, for example, [21].

We consider, in particular, the question of finding a_1 from measurements of $sU(s\theta)$ at several sufficiently large s. This question is of independent interest, but we consider this issue also for numerical testing multipoint formulas of [27] with their regularizations developed in the present work. In these numerical tests we assume for simplicity that

$$\rho(x) = \sum_{j=1}^{J} q_j \delta(x - x_j), \quad q_j \in \mathbb{R}, \quad x_j \in D. \tag{1.17}$$

The further structure of the present article is as follows. In Section 2 we recall the formulas of [27] for finding a_1 in (1.1) from z at several points, and describe related numerical algorithms. In Section 3 we recall the multipont formulas of [28] for inverse scattering at several high energies, and give analogs of these formulas for phaseless inverse scattering. In Section 4 we give further theoretical results on inverse scattering at several high energies. This includes new formulas for the reconstruction from the scattering amplitude and from boundary values of the wave functions. In Section 5, for data with random noise, we give an efficient regularization of multipoint formulas recalled in Section 2, and describe related numerical algorithm. In Section 6 we present numerical tests of the aforementioned multipoint formulas for the case of finding a_1 in (1.16)–(1.17) from $z(s) = sU(s\theta)$ given at several points s. In Section 7 we present numerical tests of the aforementioned multipoint formulas in their application to inverse scattering at several high energies. Some conclusions are summarized in Section 8.

Numerical simulations of the present work were fulfilled using Matlab.

2 Reconstruction of the leading coefficient in expansion (1.1)

In this section we recall multipoint formulas of [27] for finding a_1 in (1.1) from z given at several sufficiently large s; see formulas (2.4)–(2.7). In addition, we also describe algorithms for their numerical implementation; see Algorithms 1 and 2.

Let $z = z(s)$ be an abstract function of the form (1.1). We consider points $s_j \in (r, +\infty)$ such that

$$\begin{aligned} &s_j = s + \tau_j, \quad j = 1, ..., n, \\ &0 = \tau_1 < \tau_2 < ... < \tau_n \text{ are fixed}, \\ &\vec{\tau} := (\tau_1, ..., \tau_n), \quad 2n + 1 < N, \end{aligned} \tag{2.1}$$

or

$$\begin{aligned} &s_j = s\lambda_j, \quad j = 1, ..., n, \\ &1 = \lambda_1 < \lambda_2 < ... < \lambda_n \text{ are fixed}, \\ &\vec{\lambda} := (\lambda_1, ..., \lambda_n), \quad n = N. \end{aligned} \tag{2.2}$$

Let

$$\alpha_j(\vec{\xi}) := \prod_{i=1}^{j-1}(\xi_j - \xi_i) \quad \text{for} \quad 1 < j \le n, \quad \alpha_1(\vec{\xi}) = 1,$$
$$\beta_{n,j}(\vec{\xi}) := \prod_{i=j+1}^{n}(\xi_i - \xi_j) \quad \text{for} \quad 1 \le j < n, \quad \beta_{n,n}(\vec{\xi}) = 1, \tag{2.3}$$

where $\vec{\xi} = (\xi_1, \dots, \xi_n)$.

Then the following formulas for finding a_1 from $z(s)$ at the points s_j hold (see [27]):

$$a_1 = a_{1,n}(s, \vec{\tau}) + \mathcal{O}(s^{-n}), \text{ as } s \to +\infty, \tag{2.4}$$
$$a_{1,n}(s, \vec{\tau}) = \sum_{j=1}^{n} y_j(s, \vec{\tau}) z(s + \tau_j),$$
$$y_j(s, \vec{\tau}) = \frac{(-1)^{n-j}(s + \tau_j)^{n-1}}{\alpha_j(\vec{\tau})\beta_{n,j}(\vec{\tau})}, \quad 1 \le j \le n, \tag{2.5}$$

where s_j are defined by (2.1);

$$a_1 = a_{1,n}(s, \vec{\lambda}) + \mathcal{O}(s^{-n}), \text{ as } s \to +\infty, \tag{2.6}$$
$$a_{1,n}(s, \vec{\lambda}) = \sum_{j=1}^{n} y_j(s, \vec{\lambda}) z(\lambda_j s),$$
$$y_j(s, \vec{\lambda}) = \frac{(-1)^{n-j}\lambda_j^{n-1}}{\alpha_j(\vec{\lambda})\beta_{n,j}(\vec{\lambda})}, \quad 1 \le j \le n, \tag{2.7}$$

where s_j are defined by (2.2).

Algorithm 1: function $a_1 =$ `z_reco`(s, n, τ, z)
`// reconstruction procedure proposed in [27]`

Input:
s: minimal point
n: number of points
τ : vector of point steps $(\tau_1, ..., \tau_n)$
z: function of the form (1.1) defined in points $\{s + \tau_1, ..., s + \tau_n\}$
Output:
a_1: approximation of the first term of function z

1 $a_1 := 0$
for $j = 1..n$ **do**
2 $\quad c = (-1)^{n-j}/(\text{alpha}(j, \tau) \times \text{beta}(n, j, \tau))$
$\quad$ `// alpha, beta are defined in` (2.3)
3 $\quad a_1 = a_1 + c \times z(j) \times (s + \tau(j))^{n-1}$
end

Algorithm 2: function $a_1 = \texttt{z\_reco\_multi}(s, n, \lambda, z)$
`// reconstruction procedure proposed in [27]`

Input:
s: minimal point
n: number of points
λ : vector of point factors $(\lambda_1, ..., \lambda_n)$
z: function of the form (1.1) defined in points $\{s\lambda_1, ..., s\lambda_n\}$
Output:
a_1: approximation of the first term of function z

$a_1 := 0$
for $j = 1..n$ **do**
  $c = (-1)^{n-j}/(\text{alpha}(j, \lambda) \times \text{beta}(n, j, \lambda))$
  `// alpha, beta are defined in (2.3)`
  $a_1 = a_1 + c \times z(j) \times \lambda_j^{n-1}$
end

In connection with formulas (2.5), (2.7), note that if $\xi_{j+1} - \xi_j = \delta$, $j = 1, ..., n-1$, then

$$\alpha_j(\vec{\xi})\beta_{n,j}(\vec{\xi}) = \delta^{n-1}(j-1)!(n-j)!, \quad j = 1, ..., n. \tag{2.8}$$

Numerical examples of implementation of formula (2.4) are given in Section 6.

Remark 2.1. *For fixed s, we have that*

$$a_{1,n}(s, \vec{\tau}) = a_{1,n}(s, \vec{\lambda}), \ \textit{if } \tau_j = (\lambda_j - 1)s, \quad j = 1, ..., n. \tag{2.9}$$

We recall also that:
$y = (y_1, ..., y_n)$ in (2.5) arises as the solution of the system

$$(\gamma_i, y) = \sum_{j=1}^{n} \frac{y_j}{(s+\tau_j)^{i-1}} = \begin{cases} 1 \text{ for } i = 1, \\ 0 \text{ for } 1 < i \le n; \end{cases} \tag{2.10}$$

$y = (y_1, ..., y_n)$ in (2.7) arises as the solution of the system

$$(\gamma_i, y) = \sum_{j=1}^{n} \frac{y_j}{(\lambda_j s)^{i-1}} = \begin{cases} 1 \text{ for } i = 1, \\ 0 \text{ for } 1 < i \le n. \end{cases} \tag{2.11}$$

Here, (γ_i, y) are the scalar products of y with vectors $\{\gamma_i\}_{i=1}^n$.

3 Application to inverse scattering at high energies

In this section we recall the result of [28] consisting in application of asymptotic formulas (1.9)-(1.11) and multipoint formulas (2.4)–(2.7) to finding the Fourier transform $\widehat{v}$ from the scattering amplitude f at several sufficiently large energies; see Subsection 3.1. In addition, we also extend this result to finding $|\widehat{v}|^2$ from the differential scattering cross section $|f|^2$ at several sufficiently large energies; see Subsection 3.2.

3.1 Reconstruction of the Fourier transform in expansion (1.9)-(1.11)

Applying the abstract formulas (2.4), (2.6) to the scattering expansion (1.9)-(1.11), we have (see [28]):

$$\begin{aligned} &\widehat{v}(p) = \widehat{v}_n(p, s, \vec{\tau}) + \mathcal{O}(s^{-n}), \quad \text{as} \quad s \to +\infty, \\ &\widehat{v}_n(p, s, \vec{\tau}) = \sum_{j=1}^{n} \frac{(-1)^{n-j}(s+\tau_j)^{n-1} f(k_j(s), l_j(s))}{\alpha_j(\vec{\tau})\beta_{n,j}(\vec{\tau})}, \\ &|k_j(s)|^2 = |l_j(s)|^2 = E_j(s) = (s+\tau_j)^2, \quad s > 0, \\ &\vec{\tau} = (\tau_1, \dots, \tau_n), \ \tau_1 = 0, \ \tau_{j_1} < \tau_{j_2} \ \text{ for } \ j_1 < j_2, \end{aligned} \tag{3.1}$$

and

$$\begin{aligned}
&\widehat{v}(p) = \widehat{v}_n(p,s,\vec{\lambda}) + \mathcal{O}(s^{-n}) \ \text{ as } \ s \to +\infty,\\
&\widehat{v}_n(p,s,\vec{\lambda}) = \sum_{j=1}^{n} \frac{(-1)^{n-j}\lambda_j^{n-1} f(k_j(s), l_j(s))}{\alpha_j(\vec{\lambda})\beta_{n,j}(\vec{\lambda})},\\
&|k_j(s)|^2 = |l_j(s)|^2 = E_j(s) = (\lambda_j s)^2, \ \ s > 0,\\
&\vec{\lambda} = (\lambda_1, \dots, \lambda_n), \ \lambda_1 = 1, \ \lambda_{j_1} < \lambda_{j_2} \ \text{ for } \ j_1 < j_2,
\end{aligned} \tag{3.2}$$

where

$$k_j(s) = p + (E_j(s) - p^2)^{1/2}\omega, \ \ l_j(s) = (E_j(s))^{1/2}\omega, \tag{3.3}$$

$p \in \mathbb{R}^d$, $p \cdot \omega = 0$, $\omega \in \mathbb{S}^{d-1}$ (and ω, p are fixed), and $\alpha_j(\vec{\tau})$, $\beta_{n,j}(\vec{\tau})$ are defined in (2.3).
For $n = 1$, formulas (3.1), (3.2) reduce to (1.12). In formulas (1.12), (3.1)–(3.3) we have that

$$\begin{aligned}
&k_j(s) - l_j(s) \neq p, \ \text{ if } p \neq 0,\\
&k_j(s) - l_j(s) = p + \left((E_j(s) - p^2)^{1/2} - E_j^{1/2}(s)\right)\omega,\\
&k_j(s) - l_j(s) = p - \frac{p^2}{2\sqrt{E_j(s)}}\omega + \mathcal{O}(s^{-2}), \ \text{ as } s \to +\infty.
\end{aligned} \tag{3.4}$$

The property that $k - l = p$ is an advantage of the Born-Faddeev formulas (1.8) with respect to (1.12), (3.1), (3.2).

The Born-Faddeev formula (1.8) for fixed $E = s^2$ is considered for $|p| \leq 2s$. Formula (1.12) for fixed $s = \sqrt{E}$ is considered for $|p| \leq s$. For arbitrary n, formulas (3.1), (3.2) for fixed $s = \sqrt{E}$ are also considered for $|p| \leq s$. A larger domain for p is an advantage of (1.8) in comparison with (1.12) and (3.1), (3.2) for fixed $s > 0$.

However, a rapid convergence described by $\mathcal{O}(s^{-n})$, is the principle advantage of (3.1), (3.2), for $n \geq 2$, in comparison with (1.8), when $s \to +\infty$.

A version of formulas (3.1), (3.2) without the aforementioned disadvantage is given in Subsection 4.1.

3.2 Applications to phaseless inverse scattering

Formulas (3.1), (3.2) also have their phaseless analogs. The results can be summarized as follows:

Theorem 3.1. *Let $v \in \mathcal{C}_c^\infty(\mathbb{R}^d)$. Then*

$$\begin{aligned}
&|\widehat{v}(p)|^2 = |\widehat{v}|^{2,n}(p,s,\vec{\tau}) + \mathcal{O}(s^{-n}), \quad \text{as } \ s \to +\infty,\\
&|\widehat{v}|^{2,n}(p,s,\vec{\tau}) = \sum_{j=1}^{n} \frac{(-1)^{n-j}(s+\tau_j)^{n-1}|f(k_j(s), l_j(s))|^2}{\alpha_j(\vec{\tau})\beta_{n,j}(\vec{\tau})},\\
&|k_j(s)|^2 = |l_j(s)|^2 = E_j(s) = (s+\tau_j)^2, \ \ s > 0,\\
&\vec{\tau} = (\tau_1, \dots, \tau_n), \ \tau_1 = 0, \ \tau_{j_1} < \tau_{j_2} \ \text{ for } \ j_1 < j_2,
\end{aligned} \tag{3.5}$$

and

$$\begin{aligned}
&|\widehat{v}(p)|^{2,n} = |\widehat{v}|^{2,n}(p,s,\vec{\lambda}) + \mathcal{O}(s^{-n}) \ \text{ as } \ s \to +\infty,\\
&|\widehat{v}|^{2,n}(p,s,\vec{\lambda}) = \sum_{j=1}^{n} \frac{(-1)^{n-j}\lambda_j^{n-1}|f(k_j(s), l_j(s))|^2}{\alpha_j(\vec{\lambda})\beta_{n,j}(\vec{\lambda})},\\
&|k_j(s)|^2 = |l_j(s)|^2 = E_j(s) = (\lambda_j s)^2, \ \ s > 0,\\
&\vec{\lambda} = (\lambda_1, \dots, \lambda_n), \ \lambda_1 = 1, \ \lambda_{j_1} < \lambda_{j_2} \ \text{ for } \ j_1 < j_2,
\end{aligned} \tag{3.6}$$

where $k_j(s)$, $l_j(s)$ are defined by (3.3), and $p \in \mathbb{R}^d$, $p \cdot \omega = 0$, $\omega \in \mathbb{S}^{d-1}$ (and ω, p are fixed), and $\alpha_j(\vec{\tau})$, $\beta_{n,j}(\vec{\tau})$ are defined in (2.3).

Proof. Using (1.9) we obtain that

$$\begin{aligned}
&|f(k(s), l(s))|^2 = f(k(s), l(s))\overline{f(k(s), l(s))} = \left(\sum_{j=1}^{N} \frac{a_j(p,\omega)}{s^{j-1}} + \mathcal{O}(s^{-N})\right)\overline{\left(\sum_{j=1}^{N} \frac{a_j(p,\omega)}{s^{j-1}} + \mathcal{O}(s^{-N})\right)} =\\
&= \sum_{j=1}^{N} \frac{b_j(p,\omega)}{s^{j-1}} + \mathcal{O}(s^{-N}), \ \text{ as } s \to +\infty,
\end{aligned} \tag{3.7}$$

where

$$b_1(p,\omega) = |a_1(p,\omega)|^2, \tag{3.8}$$

and

$$b_j(p,\omega) = \sum_{k=1}^{j} a_k(p,\omega)\overline{a_{j-k+1}(p,\omega)}. \tag{3.9}$$

Formulas (3.5), (3.6) follow from (3.7) and (2.4)–(2.7).

□

4 Further theoretical results on inverse scattering at high energies

The results of this section include a variation of formulas (3.1), (3.2), (3.5), (3.6) which is considerably more convenient for numerical applications to inverse scattering at high energies. The results of this section also include formulas for inverse scattering from boundary values of the scattering wave functions ψ^+ at several large energies.

4.1 Further formulas for inverse scattering from the scattering amplitude f

Note that formulas (1.12), (3.1), (3.2), (3.5), (3.6) are not very convenient for numerical inverse scattering. The reason is that the parametrisation of k and l given by (1.10) is not very convenient. This point was already explained at the end of Subsection 3.1. However, for $v \in \mathcal{C}_c^\infty(\mathbb{R}^d)$, the following formula also holds:

$$f(k(s),l(s)) = \sum_{j=1}^{N} \frac{a_j(p,\omega)}{s^{j-1}} + \mathcal{O}(s^{-N}) \text{ as } s \to +\infty, \tag{4.1}$$

where

$$\begin{aligned} &k(s) = p/2 + (E - p^2/4)^{1/2}\omega, \quad l(s) = -p/2 + (E - p^2/4)^{1/2}\omega, \quad E = E(s) = s^2, \\ &p \in \mathbb{R}^d, \quad p \cdot \omega = 0, \quad \omega \in \mathbb{S}^{d-1}, \end{aligned} \tag{4.2}$$

and

$$a_1(p,\omega) = \widehat{v}(p), \tag{4.3}$$

where $\widehat{v}$ is defined by (1.6). In particular, due to (4.1)-(4.3), we have that

$$\widehat{v}(p) = f(k(s),l(s)) + \mathcal{O}(s^{-1}), \text{ as } s \to +\infty, \tag{4.4}$$

which follows also from (1.8).

Formulas (4.1)-(4.4) (as well as formulas (1.9)-(1.12)) follow from formula (1.5) and Propositions 2.4, 2.7 of [38] (see also, [15], [7] and other references in [38]). Note that a_j in (4.1) are different from a_j in (1.9) (in general).

In contrast with formulas (1.9)-(1.12), formulas (4.1)-(4.4) for fixed $s = \sqrt{E}$, $d \geq 2$, are considered for $|p| \leq 2\sqrt{E}$ in place of $|p| \leq \sqrt{E}$, and $k(s) - l(s) = p$ in (4.2). This is the advantage of formulas (4.1)-(4.4) in comparison with (1.9)-(1.12).

As a corollary of formulas (2.4)–(2.7) and formulas (4.1)–(4.3), we obtain the following result.

Theorem 4.1. *Let $v \in \mathcal{C}_c^\infty(\mathbb{R}^d)$. Then formulas (3.1), (3.2), (3.5), (3.6) are valid, where*

$$\begin{aligned} &k_j(s) = p/2 + (E_j - p^2/4)^{1/2}\omega, \quad l_j(s) = -p/2 + (E_j - p^2/4)^{1/2}\omega, \quad E_j = E(s_j) = s_j^2, \\ &p \in \mathbb{R}^d, \quad p \cdot \omega = 0, \quad \omega \in \mathbb{S}^{d-1}, \end{aligned} \tag{4.5}$$

in place of (3.3).

The formulas of Theorem 4.1 (as well as formulas (3.1), (3.2), (3.5), (3.6)) and inversion formulas for the Fourier transform give a method for inverse scattering from the scattering amplitude f at several large energies.

In particular, in connection with reconstruction from the Fourier transform on a ball, see [17] and references therein.

4.2 Multipoint formulas for inverse scattering from boundary values of ψ^+

Consider the scattering solutions ψ^+ satisfying (1.2), (1.3). For $v \in \mathcal{C}_c^\infty(\mathbb{R}^d)$, we have that

$$\psi^+(x,k) = e^{ikx}\left(1 + \sum_{j=1}^{N-1} \frac{b_j(x,\theta)}{s^j} + \mathcal{O}(s^{-N})\right), \text{ as } s \to +\infty, \tag{4.6}$$

$$b_1(x,\theta) = \frac{1}{2i} Dv(x,-\theta), \quad Dv(x,\theta) := \int_0^{+\infty} v(x+\tau\theta)d\tau, \tag{4.7}$$

where $x \in \mathbb{R}^d$, $s = |k|$, $\theta = k/|k|$ (x and θ are fixed). Formulas (4.6), (4.7) are well-known; see [38] and references therein. Note that Dv is known as the divergent beam transform of v; see, for example, [23].

Suppose that $supp\, v \subset \Omega$, where Ω is an open bounded convex domain in $\mathbb{R}^d$ with smooth boundary $\partial\Omega$. Let

$$\Sigma = \{(x,\theta) : x \in \partial\Omega,\ \theta \in \mathbb{S}^{d-1},\ \nu_x\theta > 0\}, \tag{4.8}$$

where ν_x denotes the outward normal to $\partial\Omega$ at point x. Then $2ib_1(x,\theta) = Dv(x,-\theta)$, $(x,\theta) \in \Sigma$, can be considered as the X-ray transform of v.

The methods for reconstructing v from its X-ray transform are developed in very details; see, for example, [23].

As a corollary of formulas (2.4)–(2.7) and (4.6), (4.7), we obtain the following result.

Theorem 4.2. *Let $v \in \mathcal{C}_c^\infty(\mathbb{R}^d)$. Let*

$$z(x,k) = 2i(e^{-ikx}\psi^+(x,k) - 1). \tag{4.9}$$

Then

$$Dv(x,-\theta) = a_{1,n}(x,\theta,s,\vec{\tau}) + \mathcal{O}(s^{-n}), \ \text{as } s \to +\infty, \tag{4.10}$$

$$a_{1,n}(x,\theta,s,\vec{\tau}) = \sum_{j=1}^{n} y_j(s,\vec{\tau}) z(x, s_j(s)\theta), \tag{4.11}$$

where s_j are defined by (2.1), y_j are defined by (2.5);

$$Dv(x,-\theta) = a_{1,n}(x,\theta,s,\vec{\lambda}) + \mathcal{O}(s^{-n}), \ \text{as } s \to +\infty, \tag{4.12}$$

$$a_{1,n}(x,\theta,s,\vec{\lambda}) = \sum_{j=1}^{n} y_j(s,\vec{\lambda}) z(x, s_j(s)\theta), \tag{4.13}$$

where s_j are defined by (2.2), y_j are defined by (2.7).

Formulas (4.9)-(4.13) are new for $n \geq 2$.

Formulas (4.9)-(4.13) and inversion formulas for the X-ray transform (see, e.g., [23]) give a method for inverse scattering from the boundary values $\psi^+(x,s\theta)$, $(x,\theta) \in \Sigma$ at several large s (that is, at several large energies).

5 Regularisation of multipoint formulas for the noisy case

Note that formulas (2.4), (2.5) and related formulas of Sections 3 and 4 are unstable with respect to random noise in z, in f and $|f|^2$, and in ψ^+, if $n \geq 2$ and s increases; see Sections 6 and 7. Formulas (2.6), (2.7) are considerably more stable in this respect. The reasons are that the coefficients $y_j(s,\vec{\tau})$ behave as

$$y_j(s,\vec{\tau}) = \mathcal{O}(s^{n-1}), \quad s \to +\infty, \tag{5.1}$$

in formulas (2.5), and as

$$y_j(s,\vec{\lambda}) = \mathcal{O}(1), \quad s \to +\infty, \tag{5.2}$$

in formulas (2.7). Therefore, the approximation $a_{1,n}$ in formulas (2.4) lose stability for large n, and also lose stability, when $\tau_{j+1} - \tau_j$ are small.

Suppose, for example, that the data z are given as $\zeta = z_{noisy}$:

$$\zeta(s) = z_{noisy}(s) = z(s) + \varepsilon N(s), \quad N(s) \sim \mathcal{N}(0,1), \tag{5.3}$$

where the random variables $N(s)$ are independent for different s, and $\mathcal{N}(0,1)$ is the normal distribution.

Below we suggest an efficient regularisation of formulas (2.4), (2.5) and also (2.6), (2.7) for the noisy case, including the model given by (5.3). In this connection, in place of $a_{1,n}$ and y_j we consider their regularised versions $a^r_{1,n}$ and y^r_j, where

$$a^r_{1,n} = \sum_{j=1}^{n} y^r_j \zeta(s_j), \tag{5.4}$$

where $s_j = s_j(s)$ is defined by (2.1) for the case of formulas (2.4), (2.5), and $s_j = s_j(s)$ is defined by (2.2) for the case of formulas (2.6), (2.7). Note that if $\varepsilon = 0$ in (5.3), then $a^r_{1,n}$ reduces to regularized reconstruction from noiseless data. Our construction of y^r is as follows.

Let π_k denote the orthogonal projection of $\mathbb{R}^n$ on the $span(\gamma_1, ..., \gamma_k)$, where γ_j are the vectors arising in (2.10) or in (2.11), and $k = 1, ..., n$.

Lemma 5.1. *Let y solve (2.10) or (2.11). Then:*

$$(\gamma_i, \pi_k y) = \begin{cases} 1 \text{ for } i = 1, \\ 0 \text{ for } 1 < i \le k; \end{cases} \tag{5.5}$$

$$\pi_1 y = \frac{\gamma_1}{n}, \quad \pi_n y = y, \tag{5.6}$$

$$\frac{1}{\sqrt{n}} = |\pi_1 y| \le |\pi_2 y| \le ... \le |\pi_n y| = |y|. \tag{5.7}$$

Proof of Lemma 5.1. Let $y^\perp_k := y - \pi_k y$. From the definition of π_k, we have that $(y^\perp_k, \gamma_j) = 0$, for $j = 1, ..., k$. Therefore, from formulas (2.10) or (2.11) we have that

$$(\gamma_i, \pi_k y) = (\gamma_i, y - y^\perp_k) = (\gamma_i, y) - (\gamma_i, y^\perp_k) = \delta^1_i, \tag{5.8}$$

where δ^j_i is the Kronecker delta. Thus, (5.5) is proved.

Next, using the definition of π_1, formula (5.5) for $k = 1$, and the fact that $\gamma_1 = (1, 1, ..., 1)$, we have that $\pi_1 y = \gamma_1/n$.

In addition, π_n is an identity operator, since $\gamma_1, ..., \gamma_n$ are linearly independent in $\mathbb{R}^n$. Thus, (5.6) is proved.

Formula (5.7) follows from (5.6) and the definition of π_k.

Lemma 5.1 is proved. □

We consider a regularisation parameter $r \in [n^{-1/2}, +\infty)$, where $r = +\infty$ corresponds to no regularization, and $r = n^{-1/2}$ corresponds to the strongest regularisation. Let

$$\mathbb{S}^{n-1}_r := \{x \in \mathbb{R}^n : |x| = r\}. \tag{5.9}$$

Let L denote the broken line defined by

$$L := \cup_{k=1}^{n-1} [\pi_k y, \pi_{k+1} y], \tag{5.10}$$

where y solves (2.10) or (2.11).

Our regularised $y^r = (y^r_1, ..., y^r_n)$ mentioned in (5.4) is defined by

$$y^r := \begin{cases} y, \text{ if } |y| \le r, \\ L \cap \mathbb{S}^{n-1}_r, \text{ if } |y| > r, \end{cases} \tag{5.11}$$

where y solves (2.10) or (2.11). This definition takes into account formula (5.7).

Computation of y^r is described in Algorithm 3 for the case of y solving (2.10). The case of y solving (2.11) is similar.

Proposition 5.2. *Suppose that assumptions (5.3), (5.4), (5.11) are fulfilled. Let*

$$m = m(y, r) = \max\{k : |\pi_k y| \le r\}. \tag{5.12}$$

Then:

$$\mathbb{D}(a^r_{1,n}) \le r^2 \varepsilon^2, \tag{5.13}$$

$$\mathbb{E} a^r_{1,n} = a_1 + \sum_{j=1}^{n} y^r_j z_m(s_j), \tag{5.14}$$

where

$$z_m(s) = z(s) - \sum_{k=1}^{m} \frac{a_k}{s^{k-1}}. \tag{5.15}$$

Due to formula (5.13), using parameter r, we control the dispersion $\mathbb{D}(a_{1,n}^r)$. The point is that without regularization (i.e., for $r = +\infty$) the dispersion $\mathbb{D}(a_{1,n}(s))$ rapidly increases when $n \geq 2$ and s increases for the case (2.5), (2.10).

In addition, for the case (2.7), (2.11), the number $m = m(y, r)$ in (5.12) is independent of s. Therefore, for this case, the error

$$\mathbb{E}(a_{1,n}^r) - a_1 = \mathcal{O}(s^{-m}), \quad s \to +\infty, \tag{5.16}$$

where m may be considerably greater than 1 for large n and not too small r.

In turn, for the case (2.5), (2.10), a proper theoretical analysis of advantages of $\mathbb{E}(a_{1,n}^r)$ in comparison with $\mathbb{E}(a_{1,1}^r)$ is more complicated and will be given elsewhere. However, we clearly see these advantages in our numerical examples.

Proof of Proposition 5.2. Using (5.3), (5.4), (5.11), we obtain that

$$\mathbb{D}(a_{1,n}^r) = \mathbb{D}\left(\sum_{j=1}^{n} y_j^r \zeta(s_j(s))\right) = \left(\sum_{j=1}^{n} (y_j^r)^2\right) \varepsilon^2 \leq r^2 \varepsilon^2. \tag{5.17}$$

From (5.3), (5.4), (5.5), (5.15) we have

$$\begin{aligned} &\mathbb{E}a_{1,n}^r = \mathbb{E}\sum_{j=1}^{n} y_j^r \zeta(s_j(s)) = \sum_{j=1}^{n} y_j^r z(s_j(s)) = \sum_{j=1}^{n} y_j^r \left(\sum_{k=1}^{m} \frac{a_k}{s_j^{k-1}} + z_m(s_j)\right) = \\ &= \sum_{k=1}^{m} a_k \sum_{j=1}^{n} \frac{y_j^r}{s_j^{k-1}} + \sum_{j=1}^{n} y_j^r z_m(s_j) = \sum_{k=1}^{n} a_k(\gamma_j, y^r) + \sum_{j=1}^{n} y_j^r z_m(s_j) = a_1 + \sum_{j=1}^{n} y_j^r z_m(s_j). \end{aligned} \tag{5.18}$$

Proposition 5.2 is proved. □

The approach based on formulas (5.4), (5.11), (5.13), (5.14) for regularising formulas (2.4)-(2.7) can be also used for the case when

$$\begin{aligned} &\zeta(s) = z^{noise}(s) = z(s) + \xi(s), \\ &\mathbb{E}\xi = 0, \text{ and } \xi(s) \text{ are independent for different } s. \end{aligned} \tag{5.19}$$

In this connection, the simplest possibility consists in replacing the dispersion ε^2 in (5.13) by

$$D = \max_{j=1\ldots n} (\mathbb{D}\xi(s_j)). \tag{5.20}$$

Algorithm 3: function $a_1 = \texttt{z\_reco\_stable}(s, n, \tau, z, r)$
`// regularized reconstruction Algorithm proposed in Section 5.`

Input:
$s > 0$: minimal point
n: number of points
$\tau = (\tau_1, ..., \tau_n)$: vector of point steps, s.t. $0 = \tau_1 < ... < \tau_n$
z: function of the form (1.1) given in points $\{s + \tau_1, ..., s + \tau_n\}$
$r \geq n^{-1/2}$: regularization parameter
Output:
$a^r_{1,n}$: stable approximation of the first term of function z

$a^r_{1,n} = 0$
`// Compute initial vector` $\vec{y}$ `defined in (2.5)`
for $j = 1..n$ **do**
  $y(j) = (-1)^{n-j}/(\text{alpha}(j, \tau) \times \text{beta}(n, j, \tau))$
  `// alpha, beta are defined in (2.3)`
  $y(j) = y(j) \times (s + \tau(j))^{n-1}$
end
`// Define vectors` $gamma\{j\}$ `arising in Lemma 5.1`
for $j = 1..n$ **do**
  for $k = 1..n$ **do**
    $gamma\{j\}(k) = 1/(s + \tau(k))^{j-1}$
  end
end
`// Compute Gram matrix for vectors` $gamma\{j\}$.
for $j = 1..n$ **do**
  for $k = 1..n$ **do**
    $G(j, k) = dot(gamma\{j\}, gamma\{k\})$
    `//` $dot(\cdot, \cdot)$ `is scalar product of vectors`
  end
end
`// Find scalar products of` y `and space vectors` $gamma\{k\}$
for $k = 1..n$ **do**
  $Ay(k) = dot(y, gamma\{k\})$
end
`// Find orthogonal projections` $P\{k\}$ `of vector` $\vec{y}$ `to subspaces` $< gamma\{1\}, .., gamma\{k\} >$
for $k = 1..n$ **do**
  `// Solve system of linear equations with matrix` G`(1:k, 1:k) and right-hand side` Ay`(1:k)`
  $Projection = \text{Solve}(G(1{:}k,\ 1{:}k),\ Ay(1{:}k))$
  `//` G`(1:k, 1:k) is k-submatrix of Gram matrix,` Ay`(1:k) is k-subvector of vector` Ay
  $P\{k\} = \sum_{j=1..k} Projection(j) \cdot gamma\{j\}$
end
Find k, s.t. $|P\{k\}| \leq r < |P\{k+1\}|$.
Find $t \in [0, 1)$, s.t. $|P\{k\}(1-t) + P\{k+1\}t| = r$.
$a^r_{1,n} = dot(P\{k\}(1-t) + P\{k+1\}t, z)$

6 Numerical examples of total charge recovering

We consider

$$z(s) = s \sum_{j=1}^{J} \frac{q_j}{|s\theta - x_j|}, \quad a_1 = \sum_{j=1}^{J} q_j, \quad \theta \in \mathbb{S}^2, \quad x_j \in \mathbb{R}^3. \tag{6.1}$$

Such functions z are of the form (1.1). In addition, z in (6.1) can be written as $z(s) = sU(s\theta)$, where U is defined by (1.15), (1.17).

For such functions z we consider the n-point reconstructions $a_{1,n}$ of a_1 defined by (2.5). We also consider the regularized reconstructions $a^r_{1,n}$ defined using formulas (5.4), (5.11). In addition, we model the noisy date using (5.3) and some other particular cases of (5.19).

Note that in order to compare n-point reconstructions $a_{1,n}$ properly for different n, we compare $\widetilde{a}_{1,n}(s) = a_{1,n}(s - \tau_n, \vec{\tau})$. The reason is that $\widetilde{a}_{1,n}(s)$ are constructed from $\{z(s-\tau_n), ..., z(s-\tau_1)\}$ with the same maximal point $s - \tau_1 = s$ for different n. Similarly, for the regularized case, we compare $\tilde{a}^r_{1,n}(s) = a^r_{1,n}(s - \tau_n, \vec{\tau})$ for different n.

Note also that numerical examples given below in Subsections 6.1 and 6.2 can be also considered as preliminary tests of n-points reconstructions $a_{1,n}$ and $a^r_{1,n}$ before much more complicated numerical problem studied in Section 7.

6.1 Simplest test

Let

$$z(s) = \frac{s}{s+1}, \quad s > 0. \tag{6.2}$$

Then $a_1 = 1$ in expansion (1.1).

Note that $z(s)$ in (6.2) arise as $z(s)$ in (6.1), where $J = 1$, $q_1 = 1$, $x_1 = (-1, 0, 0)$, $\theta = (1, 0, 0)$.

Fig. 1(a) shows the n-point reconstructions $\widetilde{a}_{1,n}(s) = a_{1,n}(s - \tau_n, \vec{\tau})$ from noiseless data $\{z(s - \tau_n), ..., z(s - \tau_1)\}$, where z is defined by (6.2), $n = 1, 2, 3$, and $\tau_j = (j - 1)$. Fig. 1(b) shows related reconstructions $\widetilde{a}_{1,n}(s)$ from noisy data $\{\zeta(s - \tau_n), ..., \zeta(s - \tau_1)\}$, where $n = 1, 2, 3$, and

$$\zeta(s) := z(s) + 0.01 \cdot N(s), \qquad \text{where } N(s) \sim \mathcal{N}(0, 1) \text{ are i.i.d. for different } s. \tag{6.3}$$

Fig. 1(a) confirms that the precision of n-point reconstructions $\widetilde{a}_{1,n}$ from the exact data increases when n increases; see Section 2 for related theoretical results. Fig. 1(b) confirms that the reconstructions $\widetilde{a}_{1,n}(s)$ from noisy data become very unstable when $n \geq 2$, and s increases; see Section 5 for related theoretical discussion.

Fig. 2(a) shows the regularized n-point reconstructions $\tilde{a}^r_{1,n}(s) = a^r_{1,n}(s - \tau_n, \vec{\tau})$ from noiseless data $\{z(s - \tau_n), ..., z(s - \tau_1)\}$, where z is defined by (6.2), $n = 1, 2, 3$, and $\tau_j = (j - 1)$. Fig. 2(b) shows the related regularized n-point reconstructions $\tilde{a}^r_{1,n}(s)$ from noisy data $\{\zeta(s - \tau_n), ..., \zeta(s - \tau_1)\}$, where $\zeta(s)$ is defined by formula (6.3). These regularized reconstructions are defined using formulas (5.4), (5.11), with $r = \sqrt{5}$.

Fig. 1(a) and Fig. 2(a) show that $\tilde{a}^r_{1,n}(s)$ converges more slowly to a_1, than $\widetilde{a}_{1,n}(s)$, for $n = 2, 3$. However, the principle advantage of $\tilde{a}^r_{1,n}(s)$ in comparison with $\widetilde{a}_{1,n}(s)$ consists in much stronger stability with respect to noise; see Fig. 1(b) and Fig. 2(b). Note that the relationship between stability and precision of $\tilde{a}^r_{1,n}(s)$ depends on r.

Note that the reconstructions $\widetilde{a}_{1,n}$ and $\tilde{a}^r_{1,n}$ shown in Fig. 1(a) and Fig. 2(a) are the mathematical expectations of the reconstructions from noisy data shown in Fig. 1(b) and Fig. 2(b), respectively.

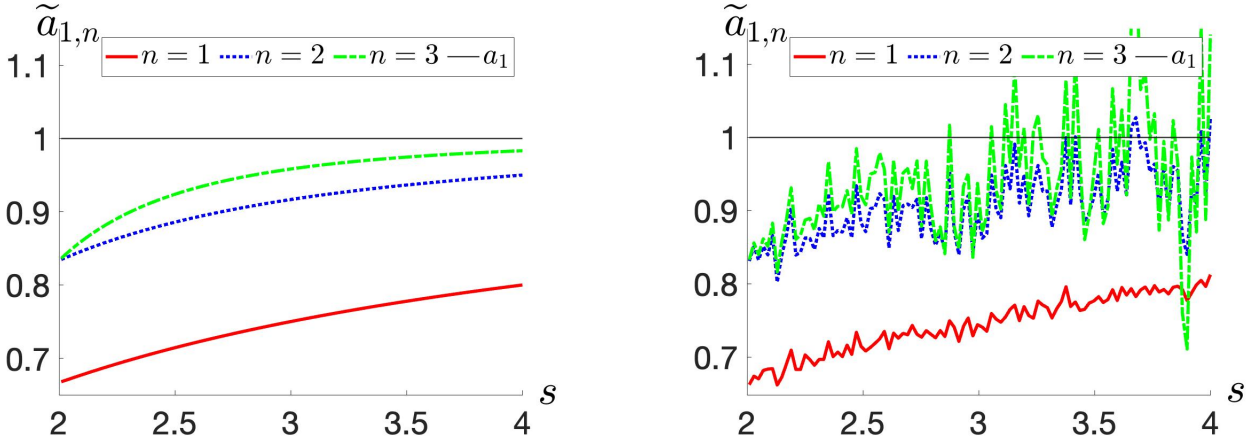

(a) Exact data. No regularization.

(b) Noisy data. No regularization.

Figure 1: n-point reconstructions $\widetilde{a}_{1,n}(s) = a_{1,n}(s - \tau_n, \vec{\tau})$ of $a_1 = 1$ for the case of z defined by (6.2) with $\tau_j = j - 1$, $j = 1, ..., n$.

(a) The case of exact data.

(b) The case of noisy data simulated using formula (6.3).

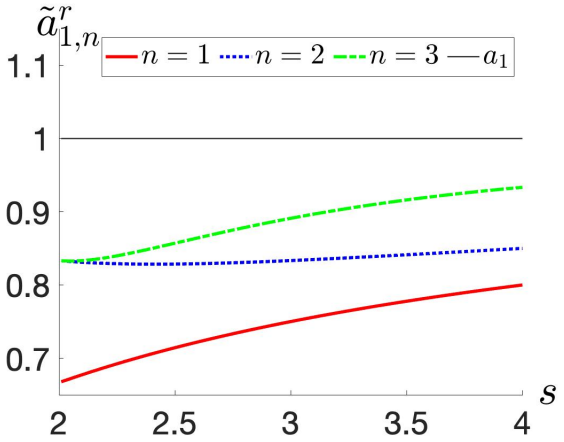

(a) Exact data. Regularization.

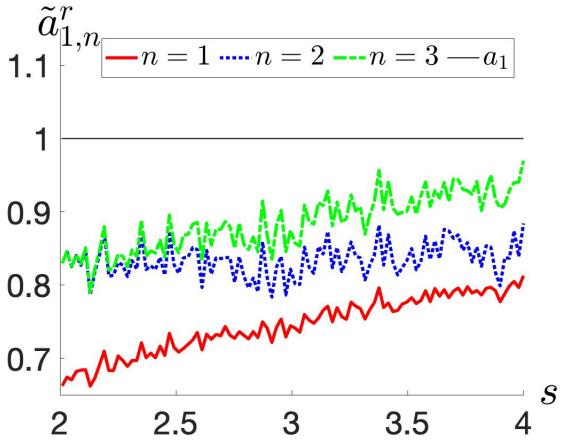

(b) Noisy data. Regularization.

Figure 2: n-point regularized reconstructions $\tilde{a}^r_{1,n}(s) = a^r_{1,n}(s-\tau_n, \vec{\tau})$ of $a_1 = 1$ for the case of z defined by (6.2) with $\tau_j = j-1$, $j = 1, ..., n$. Regularization parameter $r = \sqrt{5}$.
(a) The case of exact data.
(b) The case of noisy data simulated using formula (6.3).

6.2 Two point charge

Let z be of form (6.1), where

$$\begin{aligned} &J = 2, \qquad \theta = (1, 0, 0), \\ &q_1 = -1, \quad x_1 = (0.3669, 0.2505, -0.0518), \\ &q_2 = 2, \qquad x_2 = (0.1067, 0.2002, -0.2665). \end{aligned} \tag{6.4}$$

Then the total charge $a_1 = 1$ in expansion (1.1). This configuration can be considered as 'a dipole' with non-zero total charge.

Fig. 3(a) shows the n-point reconstructions $\widetilde{a}_{1,n}(s) = a_{1,n}(s-\tau_n, \vec{\tau})$ from noiseless data $\{z(s-\tau_n), ..., z(s-\tau_1)\}$, where z is defined by (6.1), (6.4), $n = 1, 2, 3$, and $\tau_j = (j-1)$. Fig. 3(b) shows related reconstructions $\widetilde{a}_{1,n}(s)$ from noisy data $\{\zeta(s-\tau_n), ..., \zeta(s-\tau_1)\}$, where $n = 1, 2, 3$, and

$$\zeta(s) := z(s) + 0.01s \cdot N(s), \qquad \text{where } N(s) \sim \mathcal{N}(0,1) \text{ are i.i.d. for different } s. \tag{6.5}$$

Note that the noise model (6.5) is slightly different from the noise model (6.3), but is also a partucaler case of (5.19).

Fig. 3(a) confirms that the precision of n-point reconstructions $\widetilde{a}_{1,n}$ from the exact data increases when n increases (analogously to Fig. 1(a)). Fig. 3(b) confirms that the reconstructions $\widetilde{a}_{1,n}(s)$ from noisy data become very unstable when $n \geq 2$ and s increases; this instability is even stronger than for Fig. 1(b) because of different noise model.

Fig. 4(a) shows the regularized n-point reconstructions $\tilde{a}^r_{1,n}(s) = a^r_{1,n}(s-\tau_n, \vec{\tau})$ from noiseless data $\{z(s-\tau_n), ..., z(s-\tau_1)\}$, where z is defined by (6.1), (6.4), $n = 1, 2, 3$, and $\tau_j = (j-1)$. Fig. 4(b) shows the related regularized n-point reconstructions $\tilde{a}^r_{1,n}(s)$ from noisy data $\{\zeta(s-\tau_n), ..., \zeta(s-\tau_1)\}$, where $\zeta(s)$ is defined by formula (6.5). These regularized reconstructions are defined using formulas (5.4), (5.11), with $r = \sqrt{2}$.

Fig. 3(a) and Fig. 4(a) show that $\tilde{a}^r_{1,n}(s)$ converges more slowly to a_1, than $\widetilde{a}_{1,n}(s)$, for $n = 2, 3$ (analogously to Fig. 1(a) and Fig. 2(a)). However, the principle advantage of $\tilde{a}^r_{1,n}(s)$ in comparison with $\widetilde{a}_{1,n}(s)$ consists in much stronger stability with respect to noise; see Fig. 3(b) and Fig. 4(b). This point is similar to the case of Fig. 1(b) and Fig. 2(b).

Note that the reconstructions $\widetilde{a}_{1,n}$ and $\tilde{a}^r_{1,n}$ shown in Fig. 3(a) and Fig. 4(a) are the mathematical expectations of the reconstructions from noisy data shown in Fig. 3(b) and Fig. 4(b), respectively.

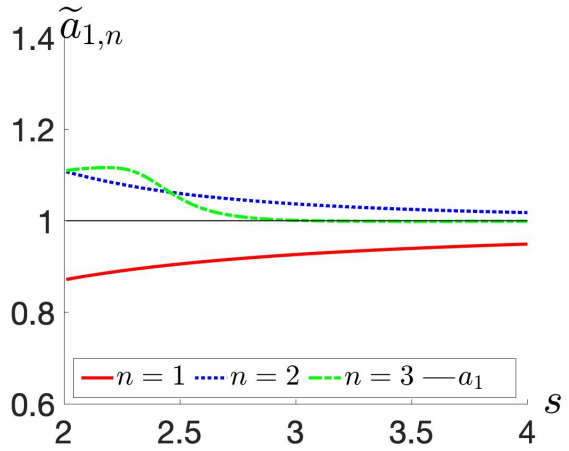

(a) Exact data. No regularization.

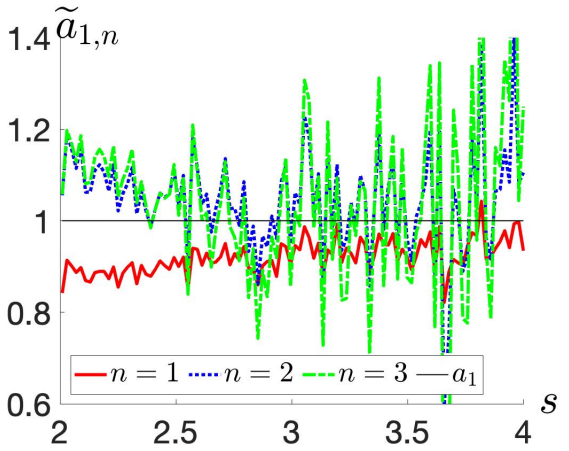

(b) Noisy data. No regularization.

Figure 3: n-point reconstructions $\widetilde{a}_{1,n}(s) = a_{1,n}(s-\tau_n, \vec{\tau})$ of $a_1 = 1$ for the case of z defined by (6.1), (6.4) with $\tau_j = j-1$, $j = 1, ..., n$.
(a) The case of exact data.
(b) The case of noisy data simulated using formula (6.5).

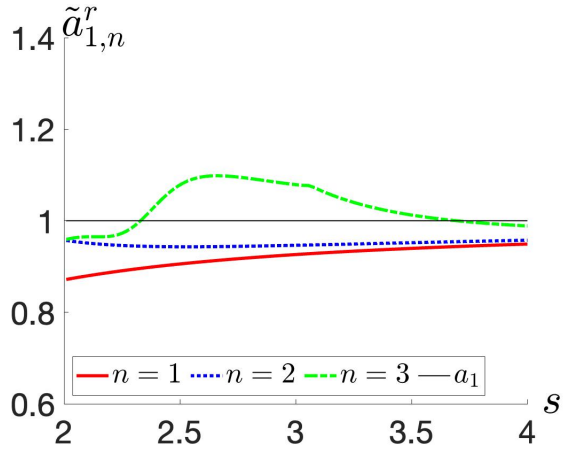

(a) Exact data. Regularization.

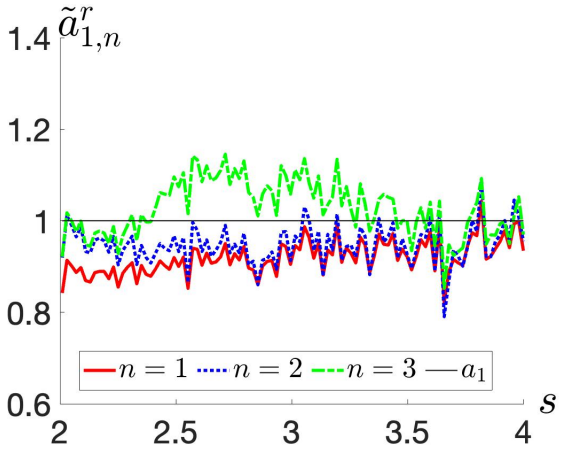

(b) Noisy data. Regularization.

Figure 4: n-point regularized reconstructions $\tilde{a}^r_{1,n}(s) = a^r_{1,n}(s-\tau_n, \vec{\tau})$ of $a_1 = 1$ for the case of z defined by (6.1), (6.4) with $\tau_j = j-1$, $j = 1, ..., n$. Regularization parameter $r = \sqrt{2}$.
(a) The case of exact data.
(b) The case of noisy data simulated using formula (6.5).

7 Numerical examples for inverse scattering

In this section we implement numerically formulas (1.13) and their phaseless analogues presented in Introduction, in Section 3, and with regularization of Section 5. More precisely, we illustrate numerically the n-point approximate reconstructions $\widehat{v}_n$ and $|\widehat{v}|^{2,n}$ defined in (3.1) and (3.5) and we illustrate numerically their regularized versions defined according to formulas (5.4), (5.11) and (5.19). We also present similar numerical results proceeding from Theorem 4.1.

In Subsection 7.1 we present some numerical preliminaries on direct scattering. In Subsection 7.2 we give numerical examples on finding the phased and phaseless Fourier transforms $\widehat{v}$ and $|\widehat{v}|^2$ from the phased and phaseless scattering amplitudes f and $|f|^2$ via the aforementioned $\widehat{v}_n$ and $|\widehat{v}|^{2,n}$. In particular, we show that this inverse scattering works better numerically when proceeding from its theoretical version given in Subsection 4.1.

7.1 Finding the scattering amplitude f

Given potential v, for finding the scattering amplitude $f = f(k, l)$ defined in (1.4), (1.10), we use the same codes as in [3, 14]. This numerical approach goes back to [37]. As in [3, 14], we consider the same Poisson noise model for $|f|^2$,

and, for simplicity, we consider the case $d = 2$.

As in [3, 14], we represent v by $\underline{v}$ defined on the space-variable grid

$$\mathcal{X}_N := \{x = \frac{4}{N}(n_1, n_2) : n_1, n_2 \in \mathbb{Z}_N\}, \tag{7.1}$$

where

$$\mathbb{Z}_N := \left\{-\frac{N}{2}, -\frac{N}{2}+1, ..., \frac{N}{2}-1\right\}, \ \ N \in 2\mathbb{N}. \tag{7.2}$$

It is also assumed that $N \geq 2\sqrt{E}/\pi$, where E is the energy in (1.2).

The main difference with [3, 14] consists in somewhat different choice of (k, l), at least, in connection with formulas (1.13), where we choose (k, l) following formula (1.10) with fixed p and ω. For the version of formulas (1.13) given in Subsection 4.1, the aforementioned difference in choice of (k, l) is considerably smaller. In any case, for simplicity, in the present work we deal with

$$\mathcal{P}_N^{int} = \{p = \frac{\pi}{2}(n_1, n_2), \ p^2 < E : \ n_1, n_2 \in \mathbb{Z}_N\}. \tag{7.3}$$

For $p \in \mathcal{P}_N^{int}$, we deal with (k, l) defined by (1.10) or (4.2), where $\omega = (-p_2, p_1)/|p|$, for $p \neq 0$, and $\omega = (-1, 0)$, for $p = 0$. The implementation of this choice of (k, l) is described in Algorithm 4.

Our numerical implementation of $\widehat{v}_n(p, s, \vec{\tau})$ in formulas (3.1) and in their version given in Subsection 4.1 is based on Algorithms 1 and 3 in Sections 2 and 5. In this implementation, $p \in \mathcal{P}_N^{int}$. Our studies include comparisons of $\widehat{v}(p)$ and $\widehat{v}_n(p, s, \vec{\tau})$.

In particular, we show that $\widehat{v}_n$, for $n = 2$ and $n = 3$, (for the case of formulas (3.1) with exact data without regularization) improves the well-known approximation $\widehat{v}_1$, when s is not too large, $\tau_{j+1} - \tau_j$ are not too small, and p is not too far from zero.

Our studies also include similar numerical implementations of $|\widehat{v}|^{2,n}(p, s, \tau)$ via formulas (3.5).

We also show that formulas (3.1), (3.5) in their version given in Subsection 4.1 lead to better numerical results.

7.2 Numerical examples

We test the n-point reconstructions $\widehat{v}_n$ and $|\widehat{v}|^{2,n}$ defined in (3.1), (3.5) and their version of Subsection 4.1 for smooth potential v shown in Figure 5(a) and Figure 5(b), where Figure 5(a) shows v itself, whereas Figure 5(b) shows $|\widehat{v}|^2$.

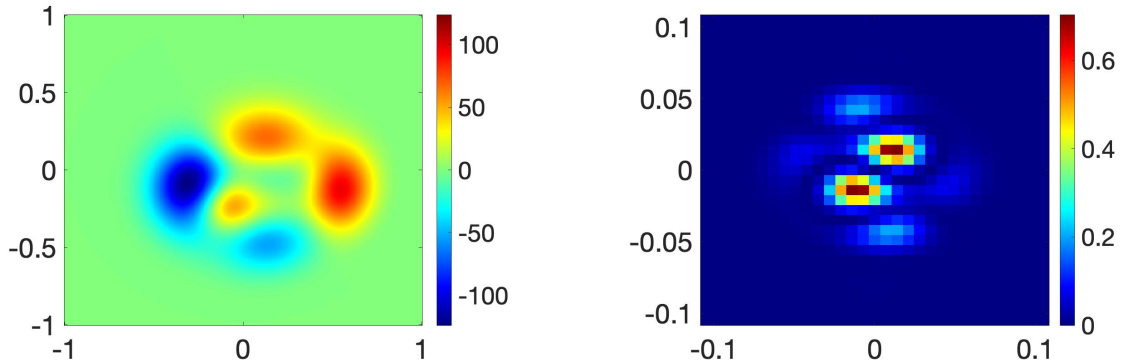

(a) (b)

Figure 5: (a) Scattering potential v. (b) Exact $|\mathcal{F}v|^2$.

For testing $\widehat{v}_n$ and $|\widehat{v}|^{2,n}$ defined in (3.1), (3.5) and their version of Subsection 4.1, we consider $n = 1, 2, 3$, $E_1 = 25^2$, $E_2 = 30^2$, $E_3 = 35^2$, and $N = 572$, where N is the grid parameter mentioned in Subsection 7.1. In particular, we have that $\tau_{j+1} - \tau_j = 5$, for $n = 2, 3$.

In a similar way with Section 6, we compare $\widehat{v}_n(p, s, \vec{\tau})$ and $|\widehat{v}(p, s, \vec{\tau})|^{2,n}$ with different s for different n, and with the same maximal energy ($E = 35^2$) involved into reconstructions.

In addition, we consider $\mathcal{P}_N^{int}$ defined by (7.3), where $E = E_1$, $N \geq 2\sqrt{E_3}/\pi$.

To measure the quality of numerical reconstructions $\widehat{v}_n$ and $|\widehat{v}|^{2,n}$, we use the relative error

$$\mathfrak{E}(u, u_0, G) = \frac{\|u - u_0\|_{\ell^2(G)}}{\|u_0\|_{\ell^2(G)}}, \tag{7.4}$$

Algorithm 4: function $[k\_directions, l\_directions] =$ `directions`$(s, N, type)$
`// the choice of proper incident and scattered directions for formula (1.10) or (4.2)`

Input:
s: current energy level $E = s^2$
N: number in $\mathcal{P}_N^{int}$
$type$: type of the grid:
$type == Melrose$ corresponds to formula (1.10), $type == Faddeev$ corresponds to formula (4.2)
Output:
$[k\_directions, l\_directions]$: set of pairs of directions $(k, l)/s$

`// list of x coordinates`
$p_1 = (\pi * N/2) * ((0 : 1 : N-1)/N - 0.5)$
`// list of y coordinates`
$p_2 = (\pi * N/2) * ((0 : 1 : N-1)/N - 0.5)$
`// define the grid of nodes with all possible coordinates`
$[P_1, P_2] = Meshgrid(p_1, p_2)$
`// find small nodes indeces`
$nodes\_index = find\_index(P_1^2 + P_2^2 < (s/2)^2)$
`//` int_nodes `corresponds to` $\mathcal{P}_N^{int}$ `of (7.3) and` p `of (1.10) or (4.2)`
$int\_nodes = [P_1(nodes\_index), P_2(nodes\_index)]$
`// list` int_nodes_ort `of vectors which are orthogonal to` int_nodes;
`//` int_nodes_ort `corresponds to` ω `of (1.10) or (4.2)`
for *k=1:length(nodes_index)* **do**
  if $P_1(nodes\_index(k))^2 + P_2(nodes\_index(k))^2 = 0$ **then**
    $int\_nodes\_ort(k) = [-1, 0]$
  else
    $int\_nodes\_ort(k) = [-P_2(nodes\_index(k)), P_1(nodes\_index(k))]/$
    $(P_1(nodes\_index(k))^2 + P_2(nodes\_index(k))^2)^{1/2}$
  end
end
`// construction of` $k\_directions$ `and` $l\_directions$ `starting from` int_nodes `and` int_nodes_ort
if $type == Melrose$ **then**
  $k\_directions = (int\_nodes + (s^2 - int\_nodes(1,:)^2 - int\_nodes(2,:)^2)^{(1/2)} * int\_nodes\_ort)/s$
  $l\_directions = int\_nodes\_ort$
else
  $k\_directions = (int\_nodes/2 + (s^2 - int\_nodes(1,:)^2/4 - int\_nodes(2,:)^2/4)^{(1/2)} * int\_nodes\_ort)/s$
  $l\_directions = (-int\_nodes/2 + (s^2 - int\_nodes(1,:)^2/4 - int\_nodes(2,:)^2/4)^{(1/2)} * int\_nodes\_ort)/s$
end

where u, u_0 are functions on some grid $G \subseteq \mathcal{P}_N^{int}$. In particular, we consider $G = \mathcal{P}_N^{small}$, where

$$\mathcal{P}_N^{small} = \{p = \frac{\pi}{2}(n_1, n_2),\ p^2 < E/4 :\ n_1, n_2 \in \mathbb{Z}_N\}. \tag{7.5}$$

The consideration of the relative error $\mathfrak{E}$ on G which is smaller than $\mathcal{P}_N^{int}$ is motivated by the fact that we cannot expect good quality of the reconstructions $\widehat{v}_n$, $|\widehat{v}|^{2,n}$ in (3.1), (3.5) near the boundary of $\mathcal{P}_N^{int}$ in view of formulas (3.4) for $|p| \approx \sqrt{E}/2$. In contrast, the approach of Subsection 4.1 overcomes this difficulty.

Note that, for simplicity, we show only $|\widehat{v}_n|^2$ for reconstructions $\widehat{v}_n$ from the scattering amplitude f at n energies $E_1, ..., E_n$, where $n = 1, 2, 3$.

Figure 6 shows reconstructions based on formulas (3.1). Recall that this involves an input data grid based on (1.10).

Figure 6(a) shows $|\widehat{v}_1(p, s, \vec{\tau})|^2$ and $|\widehat{v}|^{2,1}(p, s, \vec{\tau})$ for $s = 35$ (since $|\widehat{v}_n(p, s, \vec{\tau})|^2 = |\widehat{v}|^{2,n}(p, s, \vec{\tau})$, for $n = 1$), which is reconstructed from f at $E = 35^2$.

Figure 6(b) shows $|\widehat{v}_n(p, s, \vec{\tau})|^2$, $n = 2$, $s = 30$, which is reconstructed from f at $E = 30^2$ and $E = 35^2$.

Figure 6(c) shows $|\widehat{v}_n(p, s, \vec{\tau})|^2$, $n = 3$, $s = 25$, which is reconstructed from f at $E = 25^2$, $E = 30^2$ and $E = 35^2$.

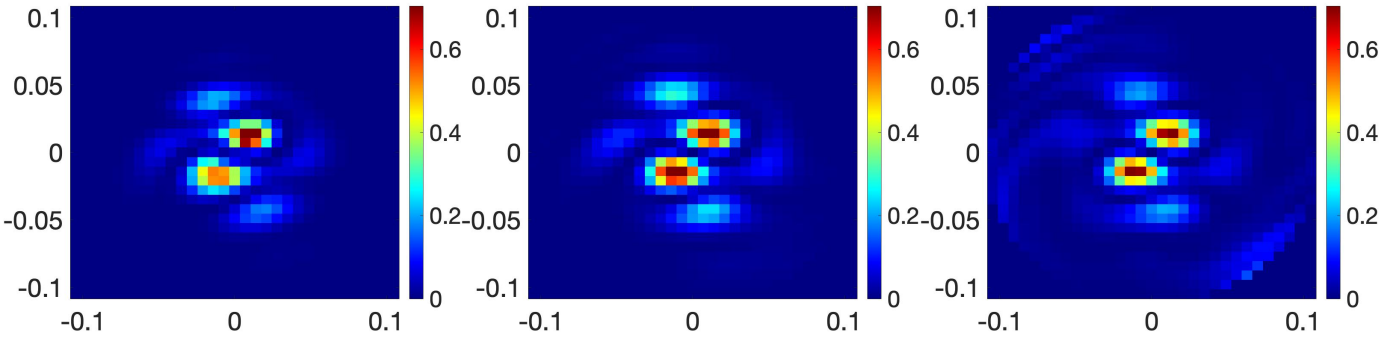

(a) (b) (c)

Figure 6: Reconstructions $|\widehat{v}_n|^2$ of $|\widehat{v}(p)|^2$ from exact phased data, where (k,l) are defined using (1.10); see Subsections 3.1, 3.2.
(a) Reconstruction $|\widehat{v}_1|^2 = |\widehat{v}|^{2,1}$ from f at $E = 35^2$.
(b) Reconstruction $|\widehat{v}_2|^2$ from f at $E = 30^2, 35^2$.
(c) Reconstruction $|\widehat{v}_3|^2$ from f at $E = 25^2, 30^2, 35^2$.

Figure 7 shows reconstructions based on formulas (3.1) in their version of Subsection 4.1. Recall that this involves an input data grid based on (4.2).

Figure 7(a) shows $|\widehat{v}_1(p,s,\vec{\tau})|^2$ and $|\widehat{v}|^{2,1}(p,s,\vec{\tau})$ for $s = 35$ (since $|\widehat{v}_n(p,s,\vec{\tau})|^2 = |\widehat{v}|^{2,n}(p,s,\vec{\tau})$, for $n = 1$), which is reconstructed from f at $E = 35^2$.

Figure 7(b) shows $|\widehat{v}_n(p,s,\vec{\tau})|^2$, $n = 2$, $s = 30$, which is reconstructed from f at $E = 30^2$ and $E = 35^2$.

Figure 7(c) shows $|\widehat{v}_n(p,s,\vec{\tau})|^2$, $n = 3$, $s = 25$, which is reconstructed from f at $E = 25^2$, $E = 30^2$ and $E = 35^2$.

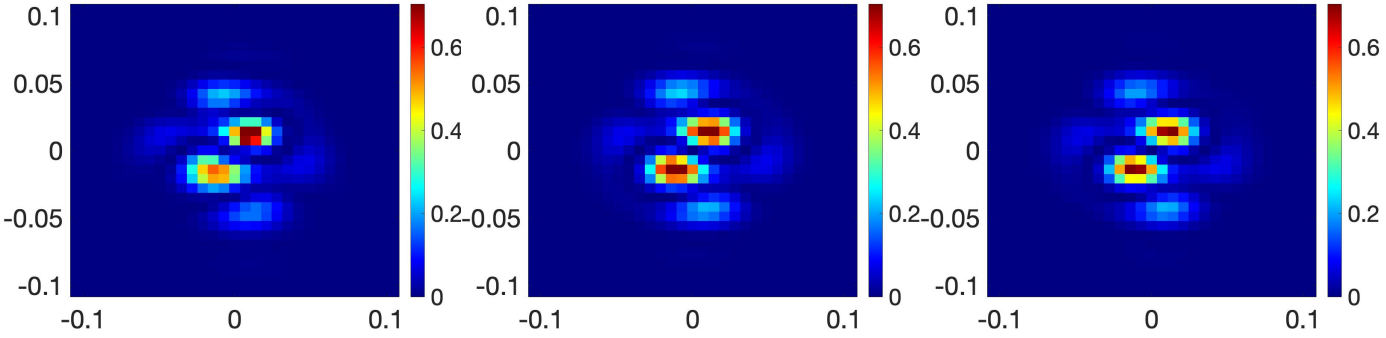

(a) (b) (c)

Figure 7: Reconstructions $|\widehat{v}_n|^2$ of $|\widehat{v}(p)|^2$ from exact phased data, where (k,l) are defined using (4.2); see Subsection 4.1.
(a) Reconstruction $|\widehat{v}_1|^2 = |\widehat{v}|^{2,1}$ from f at $E = 35^2$.
(b) Reconstruction $|\widehat{v}_2|^2$ from f at $E = 30^2, 35^2$.
(c) Reconstruction $|\widehat{v}_3|^2$ from f at $E = 25^2, 30^2, 35^2$.

For reconstructions shown in Figures 6(a), (b), (c) we have the following table of relative errors $\mathfrak{E}$ on $\mathcal{P}_N^{small}$:

j	1	2	3
$\mathfrak{E}(\widehat{v}_j, \widehat{v})$	0.3444	0.1570	0.0822
$\mathfrak{E}(\lvert\widehat{v}_j\rvert^2, \lvert\widehat{v}\rvert^2)$	0.3244	0.1979	0.0524

Table 1: Relative L_2 errors $\mathfrak{E}(\widehat{v}_j, \widehat{v})$ and $\mathfrak{E}(|\widehat{v}_j|^2, |\widehat{v}|^2)$ on $\mathcal{P}_N^{small}$ for different reconstructions $\widehat{v}_j$ of $\widehat{v}$ presented in Figure 6, where data grid parameters (k,l) are defined using (1.10).

For reconstructions shown in Figures 7(a), (b), (c) we have the following table of relative errors $\mathfrak{E}$ on $\mathcal{P}_N^{small}$:

j	1	2	3
$\mathfrak{E}(\widehat{v}_j, \widehat{v})$	0.2607	0.0840	0.0316
$\mathfrak{E}(\lvert\widehat{v}_j\rvert^2, \lvert\widehat{v}\rvert^2)$	0.2908	0.1396	0.0242

Table 2: Relative L_2 errors $\mathfrak{E}(\widehat{v}_j, \widehat{v})$ and $\mathfrak{E}(|\widehat{v}_j|^2, |\widehat{v}|^2)$ on $\mathcal{P}_N^{small}$ for different reconstructions $\widehat{v}_j$ of $\widehat{v}$ on standard grid presented in Figure 7, where data grid parameters (k, l) are defined using (4.2).

Figures 6 and 7 and the relative errors of Tables 1 and 2 show, in particular, that in our example the use of scattering amplitude f at two and three energies improves the reconstruction of $\widehat{v}$ on $\mathcal{P}_N^{small}$: $\widehat{v}_2$ is better than $\widehat{v}_1$, and $\widehat{v}_3$ is better than $\widehat{v}_2$. In addition, these reconstruction results show that the multipoint formulas in their version of Subsection 4.1 work considerably better even on small grid $\mathcal{P}_N^{small}$ than in their initial version recalled in Subsection 3.1.

Note that the reconstructions shown in Figures 6, 7 (and in Figures 8(a), (b) below) are obtained from the scattering amplitude computed numerically as described in Subsection 7.1, but without additional random noise. We consider such data as noiseless data in spite of inevitable computational errors.

Figure 8 shows reconstructions based on formulas (3.5). Recall that this involves an input data grid based on (1.10).

Figure 8(a) shows $|\widehat{v}(p, s, \vec{\tau})|^{2,n}$ for $n = 2$, $s = 30$, which is reconstructed from $|f|^2$ at $E = 30^2$ and $E = 35^5$.

Figure 8(b) shows $|\widehat{v}(p, s, \vec{\tau})|^{2,n}$ for $n = 3$, $s = 20$, which is reconstructed from $|f|^2$ at $E = 25^2$, $E = 30^2$ and $E = 35^5$.

Figures 8(c) and 8(d) show the same reconstructions as in Figures 8(a), 8(b), but from $|f|^2$ with Poisson noise. In these examples we used $N_p = 10^7$ Poisson particles per energy level.

Figures 8(e) and 8(f) show the regularized versions $|\widehat{v}(p, s, \vec{\tau})|^{2,n,r}$ of reconstructions shown in Figures 8(c), 8(d) from the same noisy data and with $r = \sqrt{10}$.

Note that $|y|^2 \approx 2000$ in formula (2.5), $n = 3$, $s = 25$, used for reconstructions of Figures 8(b), 8(d). Roughly speaking, this increases the initial dispersion in noisy values of $|f|^2$ in 2000 times. This leads to very bad reconstruction shown in Figure 8(d). In contrast, $|y^r|^2 = 10$, which is much smaller than 2000, and leads to proper result shown in Figure 8(f).

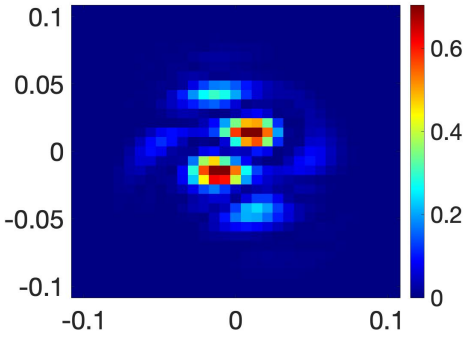

(a) Exact data. Two-point reconstruction.

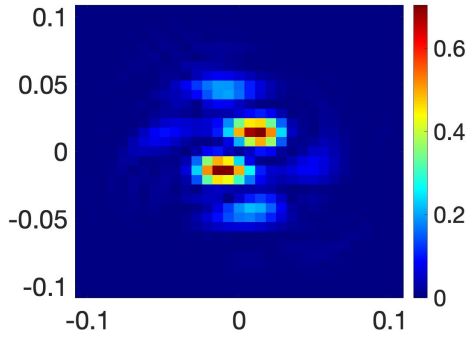

(b) Exact data. Three-point reconstruction.

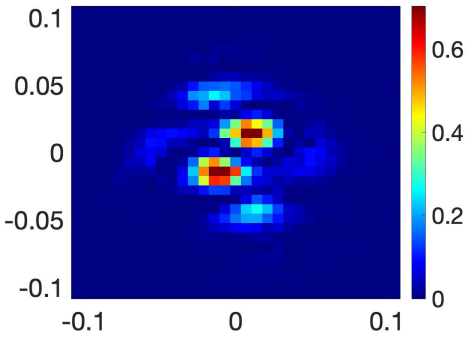

(c) Noisy data. Two-point reconstruction.

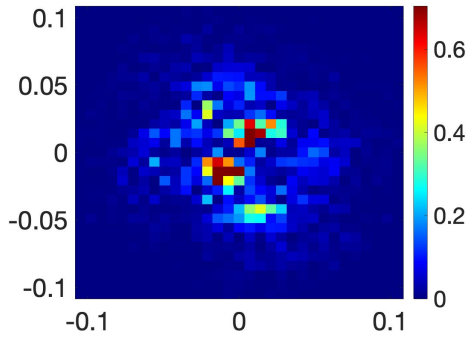

(d) Noisy data. Three-point reconstruction.

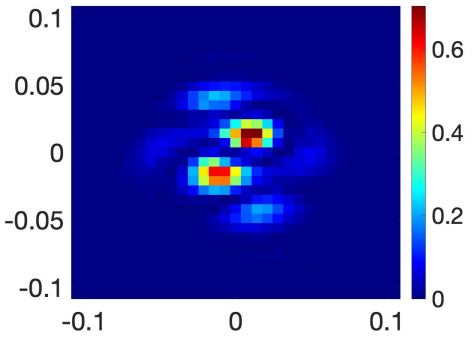

(e) Noisy data. Two-point reconstruction with regularization.

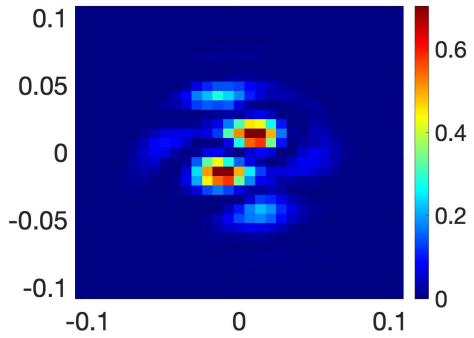

(f) Noisy data. Three-point reconstruction with regularization.

Figure 8: Reconstructions $|\widehat{v}|^{2,n}$ from exact data, $|\widehat{v}|^{2,n}_{noisy}$ from noisy data, and regularized reconstructions $|\widehat{v}|^{2,n,r}_{noisy}$ from noisy data; see Subsection 3.2, Section 5 and Subsection 7.1. Noise level: $N_p = 10^7$ per energy level. Regularized parameter $r = \sqrt{10}$.
(a) Reconstruction $|\widehat{v}|^{2,2}$ from $|f|^2$ at $E = 30^2$, 35^2. (b) Reconstruction $|\widehat{v}|^{2,3}$ from $|f|^2$ at $E = 25^2$, 30^2, 35^2.
(c) Reconstruction $|\widehat{v}|^{2,2}_{noisy}$ from noisy $|f|^2$ at $E = 30^2$, 35^2. (d) Reconstruction $|\widehat{v}|^{2,3}_{noisy}$ from noisy $|f|^2$ at $E = 25^2$, 30^2, 35^2.
(e) Regularizated reconstruction $|\widehat{v}|^{2,2,r}_{noisy}$ from noisy $|f|^2$ at $E = 30^2$, 35^2. (f) Regularizated reconstruction $|\widehat{v}|^{2,3,r}_{noisy}$ from noisy $|f|^2$ at $E = 25^2$, 30^2, 35^2.

For reconstructions shown in Figures 8(a)–(f) we have the following table of relative errors $\mathfrak{E}$ on $\mathcal{P}_N^{small}$:

j	1	2	3
$\mathfrak{E}(\lvert\widehat{v}\rvert^{2,j},\lvert\widehat{v}\rvert^2)$	0.3244	0.1691	0.0921
$\mathfrak{E}(\lvert\widehat{v}\rvert^{2,j}_{noisy},\lvert\widehat{v}\rvert^2)$	0.3226	0.2590	0.6219
$\mathfrak{E}(\lvert\widehat{v}\rvert^{2,j,r}_{noisy},\lvert\widehat{v}\rvert^2)$	0.3226	0.2468	0.1953

Table 3: Relative L_2 errors $\mathfrak{E}(|\widehat{v}|^{2,j},|\widehat{v}|^2)$ on $\mathcal{P}_N^{small}$ for different non-regularized reconstructions $|\widehat{v}|^{2,j}$ of $|\widehat{v}|^2$ from exact phaseless data, noisy phaseless data, and regularized reconstructions from noisy phaseless data, presented in Figure 8. Data grid parameters (k,l) are defined using (1.10).

For shortness of the presentation, we do not show Figures 8 in their version corresponding to results of Subsection 4.1. However, the related version of Table 3 corresponding to results of Subsection 4.1 is as follows:

j	1	2	3
$\mathfrak{E}(\lvert\widehat{v}\rvert^{2,j},\lvert\widehat{v}\rvert^2)$	0.2908	0.1269	0.0475
$\mathfrak{E}(\lvert\widehat{v}\rvert^{2,j}_{noisy},\lvert\widehat{v}\rvert^2)$	0.2895	0.1736	0.6552
$\mathfrak{E}(\lvert\widehat{v}\rvert^{2,j,r}_{noisy},\lvert\widehat{v}\rvert^2)$	0.2895	0.2186	0.1536

Table 4: Relative L_2 errors $\mathfrak{E}(|\widehat{v}|^{2,j},|\widehat{v}|^2)$ on $\mathcal{P}_N^{small}$ for different non-regularized reconstructions $|\widehat{v}|^{2,j}$ of $|\widehat{v}|^2$ from exact phaseless data, noisy phaseless data, and regularized reconstructions from noisy phaseless data. This table is a version of Table 3, corresponding to Subsection 4.1. Data grid parameters (k,l) are defined using (4.2).

Figure 6(a), Figures 8(a), (b) and the relative errors of the first lines of Tables 3 and 4 show, in particular, that in our examples the use of differential scattering cross section $|f|^2$ at two and three energies improves the reconstruction of $|\widehat{v}|^2$ on $\mathcal{P}_N^{small}$: $|\widehat{v}|^{2,2}$ is better than $|\widehat{v}|^{2,1}$, and $|\widehat{v}|^{2,3}$ is better than $|\widehat{v}|^{2,2}$.

Figures 8(c), (d) and the relative errors of the second lines of Tables 3 and 4 show that the instability of reconstructions $|\widehat{v}(p,s,\vec{\tau})|^{2,n}_{noisy}$ increases very rapidly when n increases. Note that in our example $|\widehat{v}|^{2,1}_{noisy}$ is very close to $|\widehat{v}|^{2,1}$, and, therefore, is not shown in a separated figure.

Figures 8(e), (f) and the relative errors of the third lines of Table 3 and 4 for the regularized reconstructions $|\widehat{v}(p,s,\vec{\tau})|^{2,n,r}_{noisy}$ show very good possibilities of our regularization method of Section 5 in its application to inverse scattering at high energies.

Tables 3 and 4 show that the approach of Subsection 4.1 works considerably better even on small grid $\mathcal{P}_N^{small}$.

8 Conclusion

Many functions arising in direct and inverse problems admit the asymptotic expansion of the form (1.1). In many cases, the most important information is contained in the leading coefficient a_1, which can be approximately reconstructed from z at a sufficiently large point s using the standard one-point formula

$$a_1 = z(s) + \mathcal{O}(s^{-1}), \text{ as } s \to +\infty. \tag{8.1}$$

In this work we continued studies on reconstruction of the leading coefficient a_1 in expansion (1.1) from measurements of z at *several* sufficiently large points s (multipont reconstruction approach). In particular, we presented the first numerical implementation of the recent theoretical formulas of [27] on this reconstruction. Our results include an efficient regularization of these multipoint formulas for the case of random noise.

We tested our general studies for the case of total electrical charge recovering from measurements at several remote points and for the case of inverse scattering at several high energies. In the second case, we proceed from the theoretical work [28]. We demonstrated that our numerical implementation of the aforementioned multipoint formulas essentially improves the reconstruction based on formula (8.1). We also improved and developed considerably theoretical formulas of [28] on inverse scattering at several large energies; see Section 4.

Important advantages of the aforementioned multipoint approach consist in explicit reconstruction formulas, easy and fast numerical implementation, considerable increasing in precision in comparison with (8.1) already for the two-point case, small or moderate number of measurements required for reconstruction.

In our opinion, the results of the present work open perspectives of numerical applications of the aforementioned multipoint studies to different inverse and direct problems. These issues include, in particular, further studies on:

(i) phased or phaseless inverse scattering at several high energies,
including the case of potentials v with discontinuities mentioned in Introduction;
(ii) determination of total electrical or gravitational charge from several exterior measurements;
(iii) reconstuction of far-field (scattering amplitude) from several near-field measurements;

(iv) reconstruction of phaseless far-field (scattering amplitude) from several phaseless near-field measurements;

In this respect, issues (i) and (ii) are already discussed in this work, whereas theoretical formulas for issues (iii) and (iv) are given in [27] and [32].

9 Acknowledgements

V. N. Sivkin is supported by RSF, grant № 20-11-20261, and he is fellow of the Foundation for the Advancement of Theoretical Physics and Mathematics "BASIS".

References

[1] F.V. Atkinson, *On Sommerfeld's 'radiation condition'*, London, Edinburgh Dublin Phil. Mag. J. Sci. 40 645–651 (1949)

[2] N.V. Alexeenko, V.A. Burov, O.D. Rumyantseva, *Solution of the three-dimensional acoustical inverse scattering problem. The modified Novikov algorithm,* Acoust. Phys. 54(3), 407–419 (2008)

[3] A.D. Agaltsov, T. Hohage, R.G. Novikov, *An iterative approach to monochromatic phaseless inverse scattering*, Inverse Problems 35, 24001 (24 pp.) (2019)

[4] M. Born, *Quantenmechanik der Stossvorgange*, Zeitschrift fur Physik 38 (11-12), 803-827 (1926)

[5] F.A. Berezin, M.A. Shubin, *The Schrödinger Equation*, Mathematics and Its Applications, Vol. 66, Kluwer Academic, Dordrecht (1991)

[6] V.A. Burov, N.V. Alekseenko, O.D. Rumyantseva, *Multifrequency generalization of the Novikov algorithm for the two-dimensional inverse scattering problem,* Acoust. Phys. 55(6), 843–856 (2009)

[7] V.S. Buslaev, *Trace formulas and certain asymptotic estimates of the resolvent kernel for the Schrödinger operator in three-dimensional space*, Topics in Mathematical Physics, Vol. 1, Plenum Press, Oxford (1967)

[8] K. Chadan, P.C. Sabatier, *Inverse Problems in Quantum Scattering Theory*, 2nd edn. Springer, Berlin, 1989

[9] L.D. Faddeev, *Uniqueness of the solution of the inverse scattering problem,* Vestn. Leningrad Univ. 7, 126–130 (1956) (in Russian)

[10] P.G. Grinevich, *The scattering transform for the two-dimensional Schrödinger operator with a potential that decreases at infinity at fixed nonzero energy,* Russian Math. Surveys 55(6), 1015-1083 (2000)

[11] P.G. Grinevich, R.G. Novikov, *Transmission eigenvalues for multipoint scatterers*, Eurasian Journal of Mathematical and Computer Applications 9(4), 17–25 (2021)

[12] P. Hähner, T. Hohage, *New stability estimates for the inverse acoustic inhomogeneous medium problem and applications*, SIAM J. Math. Anal. 33(3), 670-685 (2001)

[13] G.M. Henkin, R.G. Novikov, *The $\overline{\partial}$-equation in the multidimensional inverse scattering problem*, Russ. Math. Surv. 42(3), 109-180 (1987)

[14] T. Hohage, R.G. Novikov, V.N. Sivkin, *Reconstruction from differential scattering cross section with background information*, hal-03806616 (2022)

[15] W. Hunziker, *Potential scattering at high energies*, Helv. Phys. Acta 36, 838–856 (1963)

[16] M.I. Isaev, R.G. Novikov, *New global stability estimates for monochromatic inverse acoustic scattering*, SIAM J. Math. Anal. 45(3), 1495-1504 (2013)

[17] M.I. Isaev, R.G. Novikov, G. V. Sabinin, *Numerical reconstruction from the Fourier transform on the ball using prolate spheroidal wave functions,* Inverse Problems 38(10), 105002 (2022)

[18] A. Jollivet, *On inverse scattering at fixed energy for the multidimensional Newton equation in a non-compactly supported field,* Journal of Inverse and Ill-Posed Problems 21(6), 713-734 (2013)

[19] M.V. Klibanov, *Phaseless inverse scattering problems in three dimensions*, SIAM J.Appl. Math. 74(2), 392-410 (2014)

[20] M.V. Klibanov, N.A. Koshev, D.-L. Nguyen, L.H. Nguyen, A. Brettin, V.N. Astratov, *A numerical method to solve a phaseless coefficient inverse problem from a single measurement of experimental data*, SIAM J. Imaging Sci. 11(4), 2339-2367 (2018)

[21] L.D. Landau, E.M. Lifschitz, *The classical theory of fields,* Pergamon press, chapter 5.41 (1971)

[22] R.B. Melrose, *Geometric Scattering Theory. Stanford Lectures,* Cambridge University Press (1995)

[23] F. Natterer, *The Mathematics of Computerized Tomography*, Society for Industrial Mathematics, 184 pp. (2001)

[24] R.G. Novikov, *Multidimensional inverse spectral problem for the equation* $-\Delta\psi+(v(x)-Eu(x))\psi=0$, Functional Analysis and Its Applications, 22(4), 263-272 (1988)

[25] R. G. Novikov, *Small angle scattering and X-ray transform in classical mechanics,* Ark. Mat. 37, 141–169 (1999)

[26] R. G. Novikov, *An iterative approach to non-overdetermined inverse scattering at fixed energy*, Sbornik: Mathematics 206(1), 120-134 (2015)

[27] R. G. Novikov, *Multipoint formulas for scattered far field in multidimensions,* Inverse Problems 36, 095001 (2020)

[28] R.G. Novikov, *Multipoint formulas for inverse scattering at high energies,* Russ. Math. Surv. 76(4), 723-725 (2021)

[29] R. G. Novikov, *Multipoint formulas for phase recovering from phaseless scattering data*, The Journal of Geometric Analysis, 31(2), 1965-1991 (2021)

[30] R.G. Novikov, *Multidimensional inverse scattering for the Schrödinger equation*, In: Cerejeiras, P., Reissig, M. (eds) Mathematical Analysis, its Applications and Computation. ISAAC 2019. Springer Proceedings in Mathematics & Statistics, vol 385, pp 75-98, Springer, Cham. (2022)

[31] R.G. Novikov, V.N. Sivkin, *Phaseless inverse scattering with background information*, Inverse Problems 37(5), 055011 (2021)

[32] R.G. Novikov, V.N. Sivkin, *Fixed-distance multipoint formulas for the scattering amplitude from phaseless measurements*, Inverse Problems 38(2), 025012 (2022)

[33] R.G. Novikov, I.A. Taimanov, *On unitarity of the scattering operator in non-Hermitian quantum mechanics,* hal-03989986 (2023)

[34] V.G. Romanov, *Inverse problems without phase information that use wave interference*, Sib. Math. J. 59(3), 494-504 (2018)

[35] V.G. Romanov, *Phaseless problem of determination of anisotropic conductivity in electrodynamic equations*, Dokl. Math. 104(3), 385-389 (2021)

[36] A.S. Shurup, *Numerical comparison of iterative and functional-analytic algorithms for inverse acoustic scattering,* Eurasian Journal of Mathematical and Computer Applications 10(1), 79-99 (2022)

[37] G. Vainikko, *Fast Solvers of the Lippmann-Schwinger equation,* Direct and Inverse Problems of Mathematical Physics (eds R.P. Gilbert, J. Kajiwara, Y.S. Xu) Kluwer, Dordrecht (2000)

[38] D. Yafaev, *High-energy and smoothness asymptotic expansion of the scattering amplitude,* Journal of Functional Analysis 202(2), 526-570 (2003)

Roman G. Novikov, CMAP, CNRS, École polytechnique, Institut polytechnique de Paris, 91128 Palaiseau, France & IEPT RAS, 117997 Moscow, Russia
E-mail: roman.novikov@polytechnique.edu

Vladimir N. Sivkin, CMAP, CNRS, École polytechnique, Institut polytechnique de Paris, 91128 Palaiseau, France & Department of Mechanics and Mathematics, Lomonosov MSU & Center of Fundamental and Applied Mathematics, Lomonosov MSU, Moscow, 119991, Russia
E-mail: sivkin96@yandex.ru

Grigory V. Sabinin, Department of Mechanics and Mathematics, Lomonosov MSU, Moscow, 119991, Russia
E-mail: gvsabinin@gmail.com